Intense fluorescence of Au_{20}

Chongqi Yu,[1] Wolfgang Harbich,[1] Luca Sementa,[2] Luca Ghiringhelli,[3]
Edoardo Aprá,[4] Mauro Stener,[5] Alessandro Fortunelli,[2] and Harald Brune[1,*]

[1] *Institute of Physics, Ecole Polytechnique Fédérale de Lausanne (EPFL), CH-1015 Lausanne, Switzerland*
[2] *CNR-ICCOM & IPCF, Consiglio Nazionale delle Ricerche, via G. Moruzzi, 1 - 56124 - Pisa - Italy*
[3] *Fritz-Haber-Institut der Max-Planck-Gesellschaft, Faradayweg 4-6 - 14195 - Berlin - Germany*
[4] *Environmental Molecular Sciences Laboratory, Pacific Northwest National Laboratory - Richland - WA 99352 - USA*
[5] *Dip. di Scienze Chimiche e Farmaceutiche, Università di Trieste - 34127 - Trieste - Italy*

(Dated: August 25, 2017)

Ligand-protected Au clusters are non-bleaching fluorescence markers in bio- and medical applications. Here we show that their fluorescence can be an intrinsic property of the Au cluster itself. We find a very intense and sharp fluorescence peak located at λ = 739.2 nm (1.68 eV) for Au_{20} clusters in a Ne matrix held at 6 K. The fluorescence reflects the HOMO-LUMO diabatic bandgap of the cluster. Au_{20} shows a very rich absorption fine structure reminiscent of well defined molecule-like quantum levels. These levels are resolved since Au_{20} has only one stable isomer (tetrahedral), therefore our sample is mono-disperse in cluster size and conformation. Density-functional theory (DFT) and time-dependent DFT calculations clarify the nature of optical absorption and predict both main absorption peaks and intrinsic fluorescence in fair agreement with experiment.

INTRODUCTION

Gold clusters and gold nanoparticles have attracted considerable interest in fundamental research and technological applications. This started with their astonishing properties as heterogeneous catalysts [1–3] and went on with the discovery of their electronic [4] and more recently their optical properties [5, 6]. In particular, the fluorescence of Au clusters and nanoparticles has shown great potential in a variety of disciplines, such as switchable fluorescence in Au-nanoparticle/DNA/rotaxane hybrid nanostructures [7], enhanced fluorescence from dye molecules by Au nanoparticles [8], nonbleaching fluorescence of gold nanoparticles for the application in cancer cell imaging [9], multiphoton fluorescence in human insuline Au nanodots [10], molecular fluorescence of Au/SiO_2 core-shell nanoparticles [11], and label-free fluorescence on protein-protected Au clusters [12]. A fundamental understanding of the origin of fluorescence in Au nanoclusters is of critical importance for applications in bioimaging and photonics.

Since all previous studies were either performed on ligand-protected or protein-encapsulated Au clusters [12–16] it has remained unclear whether the fluorescence is intrinsic to the Au cluster or emerging from its interaction with ligands, and the considerable theoretical effort dedicated to the simulation of absorption spectra [17–21] and fluorescence [22] has not answered this question. For bare Au clusters, experiments were limited to cluster sizes below the relevant one. Absorption spectra exist only up to a size of 9 atoms [23–26] and fluorescence measurements only up to a size of 3 atoms [22, 25].

Here we report fluorescence and absorption measurements of Au_{20}. For this size the tetrahedral structure is by far the most favorable one [27] such that only this single conformer exists at our measurement temperature of 6 K. We use Ne matrices that exhibit weak van-der-Waals interactions with the clusters leading to a known offset in energies, but leaving the cluster properties unchanged with respect to the gas phase. We find that Au_{20} exhibits intense and sharp fluorescence at a wavelength of 739.2 nm (1.68 eV). This fluorescence can best be excited at 536.8 nm (2.31 eV) and 394.9 nm (3.14 eV), however also excitation in the entire UV-to-visible range leads to fluorescence. We present first-principle calculations that trace the origin of fluorescence back to molecule-like single particle excitations that are appreciably intermixed by Coulomb and spin-orbit effects. Our results prove that fluorescence is an intrinsic property of Au_{20} suggesting that in many of the above mentioned studies the fluorescence can go back to the Au core itself rather than to the ligands.

EXPERIMENTAL

We used a custom designed experimental setup to produce samples of neutral Au_{20} clusters dilutely dispersed into solid Ne matrices. For this we coupled a sputter gas aggregation cluster source [28] to a newly designed cluster ion beam line consisting of a conical octupole [29] focussing the clusters, followed by a radiofreuqency coupled quadrupole guiding them, and finally by a high mass extranuclear quadrupole for mass selection. This setup selects cluster ions up to 16000 amu with an electronically controllable mass resolution. We created a flux of Au_{20} cations with a kinetic energy of 20 eV and directed it onto a super polished aluminum mirror held at 6 K while dosing Ne that condenses onto the mirror and forms the matrix. The cluster ions are efficiently neutralized by an electron cloud formed in front of the matrix. The excess energy from the neutralization process is coupled to

* harald.brune@epfl.ch

the matrix avoiding fragmentation. The cluster flux and Ne partial pressure were adjusted to yield a cluster to rare gas atom ratio of typically $1/10^4$ optimizing signal to noise in the optical measurement while ensuring that mutual interactions between the clusters remain negligible. We grew a Au_{20}/Ne matrix with a thickness of 50 μm in 2 hours. The width of the matrix was 2 mm.

Optical absorption was measured in transmission through the 2 mm wide matrix using a deuterium or tungsten lamp as source and collecting the transmitted light with a 400 μm core optical fiber and then analyzing it in a spectrometer with a liquid-nitrogen-cooled charge coupled device as detector in a range of 250 nm to 1.0 μm (for a more detailed description see [30] . The Au_{20} absorption was obtained by subtracting a Ne matrix reference spectrum from the one of the Au_{20}/Ne matrix. For fluorescence spectra we excited with diode lasers (λ=266, 375, 473, 532 nm) normal to the surface of the Ne matrix and collected the fluorescence light perpendicular to the excitation (through the matrix) by focusing on a fiber to which the same spectrometer and detector as in the absorption spectra are attached. Excitation spectra were recorded by monochromatic detection perpendicular to the matrix at the fluorescence wavelength while varying the wavelength of the source using one of the lamps mentioned above and monochromatizing their light.

RESULTS AND DISCUSSION

A. Experiments for Au_{20}/Ne

Figure 1 shows optical absorption, excitation, and fluorescence spectra measured on mass-selected, neutral, and mono-conformal Au_{20} clusters dilutely embedded in solid Ne at 6 K. The clusters show a very rich absorption spectrum with many large and small characteristic absorption peaks that were labelled for comparison with the energies in Table 1. These peaks are superimposed onto a continuously increasing background as the energy increases. This background is consistent with the optical absorption of bulk gold [31] and inherent to basically all experimental optical spectra of ligand stabilized Au clusters at room temperature, which, apart from the Au surface plasmon, show broad structures superimposed onto that background [20, 32]. In our experiment, the spectroscopic signatures are distinct and narrow. The most prominent absorption peak occurs at 3.14 eV (395 nm, k) and the peaks of medium intensity are located at 2.31 eV (536.8 nm, b), 3.20 eV (387.5 nm, l), 3.99 eV (310.8 nm, p), 4.11 eV (301.7 nm, q), 4.52 eV (274.3 nm, t) and 5.0 eV (248 nm, u). The weak interaction with the matrix, the monodispersity, monoconformality and the low temperature clearly reveal the information on the quantum states of the cluster [35] (see theory section).

Excitation of Au_{20} at all energies above 1.8 eV results in a very intense and sharp fluorescence peak at 739.2 nm (1.68 eV) with a bandwidth (FWHM) of about

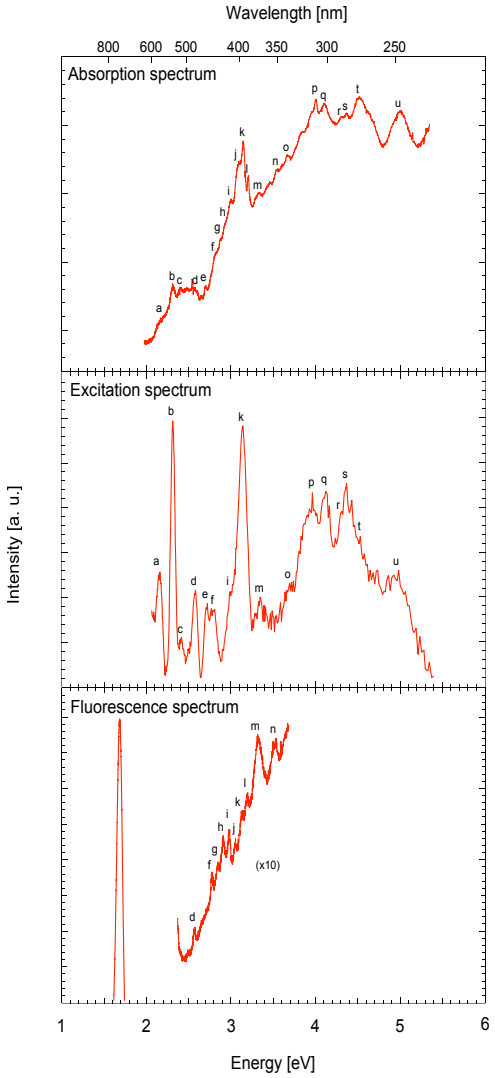

FIG. 1. a) Au_{20}/Ne absorption spectrum (broad band illumination, spectral detection). b) Excitation spectrum (monochromatic excitation, monochromatic detection at the main fluorescence line of 739.2 nm). c) Fluorescence spectrum (excitation at 266 nm, spectral detection).

35 nm (0.08 eV). Note that a group of much weaker fluorescence peaks is present. These peaks are conform to the absorption spectrum and show up only upon excitation with sufficiently high photon energy, for 266 nm see Fig. 1c, and 375 nm (not shown). Based on the observation of a strong fluorescence at 739.2 nm (1.68 eV), excitation spectra have been recorded (Fig. 1b). The main transitions associated with this fluorescence channel are at 536.8 nm (2.31 eV, b) and 395 nm (3.14 eV, k), while weaker transitions are at 574.1 nm (2.16 eV, a), 310.8 nm (3.99 eV, p), 301.7 nm (4.11 eV, q), and 284.4 nm (4.36 eV, s). Compared to the absorption spectrum, the excitation spectrum provides exactly the same positions and approximately the same line widths on all transitions, however, without the continuous background

Peaks	Energy (eV)	Wavelength (nm)
a	2.16	574.1
b	**2.31**	**536.8**
c	2.41	514.5
d	2.58	480.5
e	2.71	457.5
f	2.78	446.0
g	2.85	435
h	2.91	426
i	2.98	416
j	3.06	405
k	**3.14**	**394.9**
l	**3.2**	**387.5**
m	3.34	371.3
n	3.54	350.3
o	3.69	336.0
p	**3.99**	**310.8**
q	**4.11**	**301.7**
r	4.31	287.7
s	4.36	284.4
t	**4.52**	**274.3**
u	**5.0**	**248.0**

TABLE I. Transitions in the optical absorption of Au_{20}. Bold numbers highlight strong transitions.

absorption up to 4 eV. The excitation spectrum only mirrors the fluorescing states at 739.2 nm (1.68 eV)and therefore reflects a subset of the electronic transitions of the absorption spectrum in Fig. 1a. The missing transitions are attributed to emission dark states, *i.e.*, to non fluorescing states in the Au cluster. It is worth mentioning that very few emission dark channels are found: this is consistent with the configurational mixing deduced from TDDFT.

Assuming that the fluorescence involves the lowest excited state in the cluster, *i.e.*, there are no lower-energy emission dark channels (see discussion below), we have a precise measurement of the diabatic bandgap of Au_{20} which is 1.68 eV. This value is consistent with optical bandgaps obtained from ligand stabilized Au clusters counting only the metal core [32], *i.e.*, Au_{n-m} where n is the nominal cluster size and m the number of sulfur bonded Au atoms. It is noteworthy that the optical bandgap for the tetrahedral Au_{20} in Ne with the full valence electron count fits almost perfectly the value proposed by Jin [32] for icosaedral Au particles.

Fluorescence has so far been observed for free or quasi free Au clusters only up to the size of $n = 3$ [25, 33]. For Au_2 the fluorescence peak was at 809 nm (1.83 eV) and had a width of $\Delta E = 0.2$ eV [33], for Au_3 there were three fluorescence peaks located at 529 nm (2.34 eV), 579 nm (2.14 eV), and 809 nm (1.53 eV) [25]. Compared to the fluorescence reported for these small clusters, Au_{20} has a fluorescence peak with significantly higher intensity. Ligand stabilized Au clusters can show strong fluorescence depending on the size and the nature of the ligands [32]. For example, Wu *et al.* showed fluorescence in $Au_{25}(SCH_2CH_2Ph)^-_{18}$ at 750 nm with 150 nm linewidth [15]. Xu *et al.* found fluorescence for polydisperse Au nanoclusters on BSA (bovine serum albumin) from 650 to 700 nm with 100 nm linewidth [14]. Wen *et al.* reported fluorescence of Au_{25}/BSA at 690 nm with 120 nm linewidth [34], and finally Liu *et al.* presented fluorescence on human insuline Au nano-dots at about 700 nm with 150 nm linewidth [10]. The important and yet open question is whether the fluorescence in these ligand-protected Au nano clusters is intrinsic to the metal core or to the cluster ligand system. Our spectra on pure Au_{20} clusters show a much smaller linewidth in absorption and fluorescence. This is at least partially attributed to the low temperature of the cluster under study (T= 6K compared to 300K). It is to mention that low temperature (77K) absorption measurements on ligand stabilised Au_{144} show much narrower absorption peaks compared to the room temperature spectrum of the identical system [35]. The resemblance of our data with the ligand stabilized clusters strongly suggests that the fluorescence found in the biologically relevant systems can be Au mediated.

B. DFT and TDDFT modeling and comparison with experiment

A first-principles-based theoretical investigation of fluorescence of Ne-embedded gold clusters represents a difficult computational task, due to the interplay of several physical effects: mixing of molecule-like and preplasmonic excitations, spin-orbit coupling, influence of Ne matrix, role of van der Waals (vdW) dispersion interactions, crossing of potential energy surfaces of different excited states. To face this challenge we adopt a combination of different methods and codes.

We focus first on the long-standing problem of quantifying the effect of the Ne matrix on the structure and optical properties of embedded Au clusters. For this we considered (i) tetrahedral (T_d) Au_{20} and (ii) a $Au_{20}Ne_{100}$ cluster with the 100 Ne atoms arranged according to a homomorphic tetrahedral layer surrounding Au_{20}. We relaxed the structure using density-functional theory (DFT) employing a generalized-gradient-approximation Perdew-Burke-Ernzerhof (PBE) exchange-correlation (xc-)functional [36]. VdW interactions were introduced by adding to the DFT energy a sum over $C_6[n]/R^6$ tails, with C_6 coefficients derived in two different ways: either via the Tkatchenko-Scheffler (vdW-TS) scheme, *i.e.*, from the self-consistent electron density and reference values for the free atoms [37], or via the more recent range-separated many-body dispersion (MBD) approach [38]. The accuracy of the vdW-TS approach for predicting the structural properties of Au clusters interacting with rare-gas atoms has been validated against higher-level first-principle methods and experiment [39], and represents the current state-of-the-art modeling of such systems. The MBD approach is more recent and has been shown to be in general superior to the vdW-TS approach, in particular for heterogenous systems. This can be understood because MBD includes

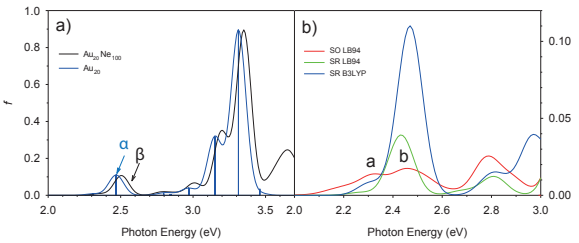

FIG. 2. TDDFT-simulated absorption spectrum of Au_{20} and $Au_{20}Ne_{100}$ at the DFT/PBE-MBD geometries: a) Au_{20} (both discrete and smoothed, blue line) and $Au_{20}Ne_{100}$ (smoothed, black lines) using the B3LYP xc-functional at scalar-relativistic (SR) level; b) Au_{20} using: B3LYP at scalar-relativistic (SR) level (smoothed, blue line), LB94 xc-functional at SR level (smoothed, green line), and LB94 xc-functional including spin-orbit (SO) coupling (both discrete and smoothed, red lines). In a) the α and β SR peaks on which fluorescence has been explicitly simulated are indicated, while in b) the peaks indicated as a and b correspond to the assignment of the corresponding experimental absorption features. Smoothed profiles are obtained by convolution with Gaussian functions of FWHM=0.12 eV. Note that the photon energy range is different in a) and b) panels to better highlight the broadening due to SO coupling in the region below 3 eV.

many-body contributions and the self-consistent screening of the atomic polarizability. The FHI-aims package [40] was used in these calculations, and the optimized geometries at the PBE-MBD level are reported in the Supplementary Information, SI (the PBE-vdW-TS geometries and associated TDDFT spectra turn out to be very similar so they are not explicitly reported). As a major conclusion of this analysis, the effect of the Ne matrix on the geometry of Au_{20} in the electronic ground state turns out to be negligible, with differences in coordinate values less than 0.01 Å.

The optical absorption spectra of Au_{20} and $Au_{20}Ne_{100}$ were then simulated at the optimised DFT/PBE-MBD geometries via time-dependent DFT (TDDFT) calculations in the Casida formalism [41] using the hybrid B3LYP xc-functional [42] at the scalar-relativistic (SR) level, and the results are reported in Fig. 2a. Previous theoretical work showed that the position and intensity of predicted absorption peaks of Au_{20} are rather sensitive to the theoretical approach employed, especially the xc-functional [43]. Local density or gradient-corrected xc-functionals severely underestimate the intensity of absorption peaks below 3 eV, and a proper description of the Coulombic tail of the potential is crucial to assure a reasonable description of the optical response of Au clusters [43]. Neglecting for the moment spin-orbit (SO) effects, TDDFT/B3LYP predicts absorption peaks below 3 eV at 2.22 eV, 2.42 eV, and 2.88 eV, and three major peaks between 3.08 and 3.39 eV towering the spectrum (see Table S1 of the SI for more information and an analysis of the excited states in terms of single-particle components). Figure 2a demonstrates that the effect of the Ne matrix on the absorption of Au_{20} is minor, basically amounting to a small blue-shift of the peak positions (a charge compression effect on the excited orbitals). Note that for computational reasons the number of calculated roots of the Casida matrix, thus the range of excitation energies, is limited. The TDDFT/B3LYP calculations in Fig. 2a are performed using a double-zeta-plus-polarization basis set and the NWChem package [44] at the SR level.

To better understand the nature of the low-lying excited electronic states, we report in Fig. 3 the single-particle orbitals of Au_{20} in its electronic SR ground state as a function of energy and occupation, labeled according to the irreducible representations of the T_d symmetry group (more details are provided in Table S1 and Fig. S1 of the SI where the orientation of Au_{20} used to plot orbital densities is shown). We then highlight in particular the two lowest excited states at 2.22 eV and 2.42 eV, respectively, that are explicitly indicated as α and β both in Fig. 3 and in Fig. 2a, and mainly correspond to $16e \rightarrow 30t2$ and $29t2 \rightarrow 30t2$ single-particle transitions (see Table S1).

Spin-orbit (SO) effects are known to be potentially important in the optical response of Au clusters [45]. Being unable to include SO coupling in the B3LYP calculations for technical reasons, we estimate its influence by using the semi-local Coulomb-tail-corrected SAOP xc-functional [46] and the ADF package [47]. Although SAOP is less accurate than B3LYP or other hybrid xc-functionals, SAOP predicts for Au_{20} an optical absorption profile qualitatively consistent with these xc-functionals. The SAOP absorption spectra up to 3 eV with and without SO coupling are reported in Fig. 2b. As expected, the SR peaks split into several peaks after the introduction of SO coupling, thus producing an overall spectral appearance in good agreement with the rich experimental absorption shown in Fig. 1a, whose continuous background is so interpreted as due to SO splitting of SR absorption intensity into a multitude of peaks.

Moreover, by comparison with Fig. 1a and Table 1, we can single out SO features in Fig. 2b that can be associated to the (a) and (b) experimental peaks. These SO features derive basically from a mixing of the SR peaks at 2.22 eV and 2.42 eV, respectively, while the experimental major peaks (j,k,l) can analogously be put into correspondence with features deriving from the three major SR peaks between 3.08 and 3.39 eV.

In summary, the comparison between observed and simulated absorption spectra demonstrates that (i) the Ne matrix does not qualitatively influence structure and electron dynamics in Au_{20}, and (ii) the generally fair agreement between TDDFT predictions (including previous literature [43]) and experiment makes us confident in using a TDDFT approach also for investigating fluorescence phenomena. For technical reasons we are only able to do this at the TDDFT/B3LYP scalar-relativistic (SR) level on the two low-energy α and β absorption peaks.

We thus investigate the evolution/relaxation of the

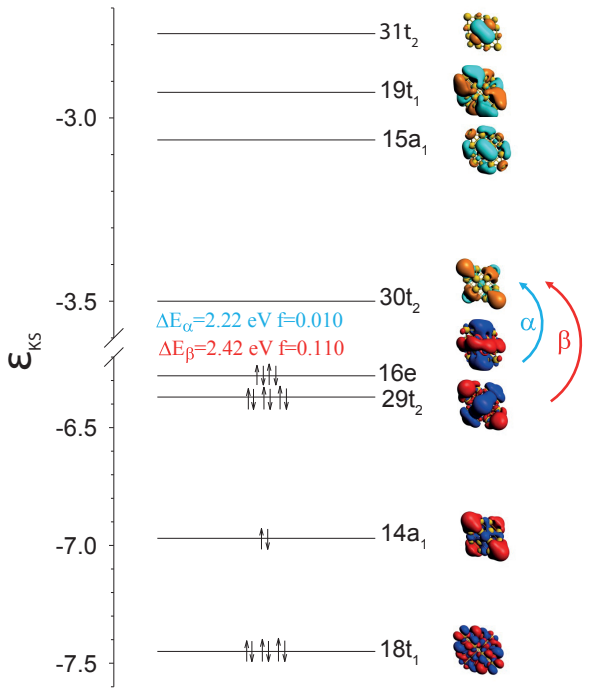

FIG. 3. Au_{20} DFT/B3LYP single-particle molecular orbitals as a function of energy and occupation, labeled according to the irreducible representations of the T_d symmetry group. The main single-particle components of the two lowest-energy TDDFT/B3LYP excited states at the scalar-relativistic (SR) level with their excitation energy and oscillator strength are also indicated with blue and red arrows for the α and β excitation, respectively.

first two α and β excited states of bare Au_{20}, *i.e.*, the very weak transition at 2.22 eV (named α and β) and the more intense absorption at 2.42 eV (named α and β). We recall that these SR states originates SO states that can be put into correspondence with (a,b)-peaks at 2.31 eV in the experimental excitation spectrum of Figure 1b. The geometry of these two excited states has been relaxed at the TDFFT/B3LYP level using the NWChem code. At the T_d equilibrium ground state geometry, both α and β are three-fold-degenerate electronic states belonging to the t_1 irreducible representation of the T_d symmetry group. An analysis of the eigenvector of the Hessian matrix more strongly coupled to energy minimization shows that α relaxes its energy by lowering the symmetry from T_d to D_2, smoothly ending up in a local energy minimum in which the excitation energy from the electronic ground state is 1.99 eV (the Cartesian coordinates of the relaxed geometry are reported in the SI). β initially relaxes its energy by lowering the symmetry from T_d to C_2. However, after an initial decrease in energy by ≈ 0.1 eV, the minimization process gets trapped in regions of the potential energy surface exhibiting a complicated crossing of excited states and conical intersections (the Cartesian coordinates of one of these crossing geometries are reported in the SI). Notably, in these regions excited states originating from components of the α and β triply degenerate multiplets appreciably mix, with mixing coefficients (*i.e.*, expansion coefficients of β-like excited states onto single-particle excitations originally pertaining to α-like excited states and vice versa) ranging from 0.1 to 0.3. It is therefore reasonable to assume that surface hopping from β-like to α-like excited states easily occurs in these regions, followed by a smooth relaxation to the D_2 local minimum of the lowest-energy E_1-like component, which finally fluoresces into the electronic ground state. It can be noted that the weaker oscillator strength of α-like states delays spontaneous fluorescent emission. We thus finally predict a shift between β absorption at 2.42 eV and α fluorescence of 0.43 eV, in fair agreement with experimental observations.

CONCLUSION

We present the first optical absorption, excitation, and fluorescence spectra of the tetrahedral Au_{20}. In our experiments, Au_{20} is embedded in a solid neon matrix at 6 K. Our first-principles calculations reveal that this matrix has no effect on the cluster structure, its only effect is a slight blue shift of the absorption spectrum. The absorption spectrum exhibits a series of sharp discrete transitions on a smooth background that increases with energy and whose overall appearance is similar to the background found for ligand-protected Au clusters at low temperatures. Au_{20} exhibits intense and sharp fluorescence. Our results strongly suggest that the metal core in ligand-protected clusters plays a central role in the fluorescence. The fluorescence in Au_{20} is shown to involve mostly HOMO-LUMO and HOMO(-1)-LUMO excitations, which are well separated in the tetrahedral ground-state geometry, but strongly interact and mix when excited-state relaxation deforms it. It is finally notable that fluorescence emission – as shown by TDDFT response calculations – involves the lowest excited state, (*i.e.*, there are no energetically lower dark emission channels). Therefore the fluorescence peak provides a precise measure of the diabatic bandgap which is 1.68 eV for Au_{20}.

SUPPLEMENTARY MATERIAL

The supplementary material provides additional information on the optical absorption excitations of Au_{20} in terms of single-particle components and associated induced-density plots and the geometry of Au_{20} and $Au_{20}Ne_{100}$ systems in their electronic ground and two lowest excited states.

ACKNOWLEDGEMENTS

Experimental work has been supported by the Swiss National Science Foundation. Computational research was performed in part using EMSL, a DOE Office of Science User Facility sponsored by the Office of Biological and Environmental Research and located at Pacific Northwest National Laboratory, and PNNL Institutional Computing at Pacific Northwest National Laboratory. Support from CINECA supercomputing centre within the ISCRA program is also gratefully acknowledged.

[1] M. Haruta, N. Yamada, T. Kobayashi, and S. Iijima, J. Cat. **115**, 301 (1989).
[2] M. Valden, X. Lai, and D. W. Goodman, Science **281**, 1647 (1998).
[3] M. Haruta, Nature **437**, 1098 (2005).
[4] C. Zhang, Y. He, H. P. Cheng, Y. Q. Xue, M. A. Ratner, X. G. Zhang, and P. Krstic, Phys. Rev. B **73**, 125445 (2006).
[5] T. G. Schaaff and R. L. Whetten, J. Phys. Chem. B **104**, 2630 (2000).
[6] P. Zhang, X. Yang, Y. Wang, N. Zhao, Z. Xiong, and C. Huang, Nanoscale **6**, 2261 (2014).
[7] A. Cecconello, C.-H. Lu, J. Elbaz, and I. Willner, Nano Lett. **13**, 6275 (2013).
[8] J. H. Guo, L. Z. Liu, X. B. Zhu, X. L. Wu, and P. K. Chu, Appl. Phys. Lett. **104**, 141910 (2014).
[9] H. He, C. Xie, and J. Ren, Anal. Chem. **80**, 5951 (2008).
[10] C.-L. Liu, T.-M. Liu, T.-Y. Hsieh, H.-W. Liu, Y.-S. Chen, C.-K. Tsai, H.-C. Chen, J.-W. Lin, R.-B. Hsu, T.-D. Wang, C.-C. Chen, C.-K. Sun, and P.-T. Chou, Small **9**, 2103 (2013).
[11] P. Reineck, D. Gomez, S. H. Ng, M. Karg, T. Bell, P. Mulvaney, and U. Bach, ACS Nano **7**, 6636 (2013).
[12] Y. Wang, Y. Wang, F. Zhou, P. Kim, and Y. Xia, Small **8**, 3769 (2012).
[13] S. Wang, X. Meng, A. Das, T. Li, Y. Song, T. Cao, X. Zhu, M. Zhu, and R. Jin, Angew. Chem. Int. Ed. **53**, 2376 (2014).
[14] Y. Xu, J. Sherwood, Y. Qin, D. Crowley, M. Bonizzoni, and Y. Bao, Nanoscale **6**, 1515 (2014).
[15] Z. Wu and R. Jin, Nano Letters **10**, 2568 (2010).
[16] X. Wen, P. Yu, Y.-R. Toh, X. Ma, S. Huang, and J. Tang, Nanoscale **5**, 10251 (2013).
[17] C. M. Aikens, J. Phys. Chem. A **113**, 10811 (2009).
[18] S. Malola, L. Lehtovaara, J. Enkovaara, and H. Hï¿½kkinen, ACS Nano **7**, 10263 (2013).
[19] J. C. Idrobo, W. Walkosz, S. Yip, S. Oeguet, J. Wang, and J. Jellinek, Phys. Rev. B **76**, 205422 (2007).
[20] H. C. Weissker, H. B. Escobar, V. D. Thanthirige, K. Kwak, D. Lee, G. Ramakrishna, R. L. Whetten, and X. López-Lozano, Nat. Communic. **5**, 3785 (2014).
[21] G. Barcaro, L. Sementa, A. Fortunelli, and M. Stener, Phys. Chem. Chem. Phys. **17**, 27952 (2015).
[22] K. L. Dimuthu, M. Weerawardene, and C. M. Aikens, J. Am. Chem. Soc. **138**, 11202 (2016).
[23] G. A. Bishea and M. D. Morse, J. Chem. Phys. **95**, 5646 (1991).
[24] W. Harbich, S. Fedrigo, J. Buttet, and D. Lindsay, Zeitschr. Phys. D **19**, 157 (1991).
[25] S. Fedrigo, W. Harbich, and J. Buttet, J. Chem. Phys. **99**, 5712 (1993).
[26] S. Lecoultre, A. Rydlo, C. Felix, J. Buttet, S. Gilb, and W. Harbich, J. Chem. Phys. **134**, 074302 (2011).
[27] J. Li, X. Li, H. J. Zhai, and L. S. Wang, Science **299**, 864 (2003).
[28] I. M. Goldby, B. von Issendorff, L. Kuipers, and R. E. Palmer, Rev. Sci. Instrum. **68**, 3327 (1997).
[29] M. A. Rottgen, K. Judai, J. M. Antonietti, U. Heiz, S. Rauschenbach, and K. Kern, Rev. Sci. Instrum. **77**, 013302 (2006).
[30] F. Conus, J. T. Lau, V. Rodrigues, and C. Félix, Rev. Sci. Instrum. **77**, 113103 (2006).
[31] P. B. Johnson and R. W. Christy, Phys. Rev. B **6**, 4370 (1972).
[32] R. Jin, Nanoscale **7**, 1549 (2015).
[33] S. Lecoultre, A. Rydlo, C. Félix, and W. Harbich, Eur. Phys. J. D **52**, 187 (2009).
[34] X. Wen, P. Yu, Y. Toh, A. Hsu, Y. Lee, and J. Tang, J. Phys. Chem. C **116**, 19032 (2012).
[35] H. C. Weissker, H. B. Escobar, V. D. Thanthirige, K. Kwak, D. Lee, G. Ramakrishna, R. L. Whetten, and X. Lopez-Lozano, NATURE COMMUNICATIONS **5** (2014), 10.1038/ncomms4785.
[36] J. P. Perdew, K. Burke, and M. Ernzerhof, Phys. Rev. Lett. **77**, 3865 (1996).
[37] A. Tkatchenko and M. Scheffler, Phys. Rev. Lett. **102**, 073005 (2009).
[38] A. Ambrosetti, A. M. Reilly, R. A. DiStasio, and A. Tkatchenko, J. Chem. Phys. **140**, 202086 (2014).
[39] L. M. Ghiringhelli, P. Gruene, J. T. Lyon, D. M. Rayner, G. Meijer, A. Fielicke, and M. Scheffler, N. J. Phys. **15**, 083003 (2013).
[40] V. Blum, R. Gehrke, F. Hanke, P. Havu, V. Havu, X. Ren, K. Reuter, and M. Scheffler, Comp. Phys. Communic. **180**, 2175 (2009).
[41] M. Casida, "Recent advances in density-functional methods," (World Scientific, 1995) p. 155.
[42] A. D. Becke, J. Chem. Phys. **98**, 5648 (1993).
[43] B. Anak, M. Bencharif, and F. Rabilloud, RSC Adv. **4**, 13001 (2014).
[44] R. A. Kendall, E. Aprà, D. E. Bernholdt, E. J. Bylaska, M. Dupuis, G. I. Fann, R. J. Harrison, J. Ju, J. A. Nichols, J. Nieplocha, T. P. Straatsmab, T. L. Windus, and A. T. Wong, Comp. Phys. Comm. **128**, 260 (2000).
[45] D. Jiang, M. Kühn, Q. Tang, and F. Weigend, J. Phys. Chem. Lett. **5**, 3286 (2014).
[46] O. Gritsenko, P. Schipper, and E. Baerends, Chem. Phys. Lett. **302**, 199 (1999).
[47] C. F. Guerra, J. G. Snijders, G. te Velde, and E. J. Baerends, Theor. Chem. Acc. **99**, 391 (1998).